Article:
Ramadhan, AA orcid.org/0000-0002-0711-572X, Kapur, N orcid.org/0000-0003-1041-8390, Summers, JL et al. (1 more author) (2017) Numerical Analysis and Optimization of Miniature Electrohydrodynamic Air Blowers. IEEE Transactions on Plasma Science, 45 (11). pp. 3007-3018. ISSN 0093-3813

https://doi.org/10.1109/TPS.2017.2755365

Numerical Analysis and Optimization of Miniature Electrohydrodynamic Air Blowers

Abdulmajeed A. Ramadhan, N. Kapur, J.L. Summers, H.M. Thompson

***Abstract*— As the demand for advanced microelectronic devices of small form factor and high power density has increased, the capability of the miniaturized mechanical solutions for effective cooling has become critical. Electrohydrodynamic (EHD) air blowers have great potential as alternative cooling solutions over the traditional mechanical systems to meet the thermal management requirements with flexible design and considerable flow production for effective heat removal. In the present work, a numerical analysis and optimization of wire-to-plane EHD air blowers are performed based on 2D developed models validated against previous data. For a range of blower heights from 2 to 10 mm, the location and length of the collecting plane located at the blower walls apart from the emitter wire electrode are investigated and optimized based on pumping efficiency using ranges of fixed operating powers and voltages. Simple relations for each optimization method are presented to determine the optimal blower configuration. Results of flow rate and static pressure obtained by each optimized blower show good agreement with those predicted by EHD scaling laws previously presented.**

***Index Terms*— Electrohydrodynamic (EHD) flow, Ionic wind pumps, Numerical analysis, Design optimization.**

I. Introduction

EFFICIENT cooling of microelectronic components has become a critical issue in thermal management as the demand for small form factor and high power density consumer electronics is steadily increasing. This has resulted in advanced developments of thermal solutions in order to make them compact and efficient in heat removal with low levels of acoustic noise and power consumption. For decades, mechanical systems such as axial fans and centrifugal blowers have been successfully used for cooling microelectronic applications and consumer devices due to their efficiency in heat dissipation, low manufacturing cost and ease of installation [1]. However, although today's industries offer miniaturized structures of rotary fans with thicknesses in millimeters, further shrinkage in their size, which is practically limited by the fan blade height and motor design, leads to less reliability, more complex manufacturing challenges, a reduction in the flow generation, and an increase in acoustic level due to the associated high rotational speed [2-4]. Moreover, it has been demonstrated that the traditional fan laws are not effective at low Reynolds number flows to predict the flow characteristics of miniature axial [5, 6] and centrifugal [7, 8] fans, where the viscous effects become considerable. A recent analysis showed that the predicted performance of the miniaturized rotary centrifugal fans, which are usually used in thin electronic applications, under the scaling laws does not exactly agree with that of experiments in terms of flow rate, maximum pressure rise, and power consumption [9]. Due to these challenges, the need for effective miniature cooling solutions that meet the thermal management requirements for small form factor applications such as notebooks has become essential.

In their comprehensive review and comparison study, Wang et al. [1] recently concluded that electrohydrodynamic (EHD) air movers have great potential as a novel thermal management solution for microelectronics cooling based on performance compared to other alternative air pumping methods such as piezoelectric fans and synthetic jets. Moreover, they found that EHD air pumps offer important advantages over traditional rotary fans due to their silent operation, reduced power consumption, flexible structure, smaller volume requirements and higher heat transfer performance on small form factor applications.

EHD flow is a process of interactions between electric fields and fluids, resulting in air motion (called ionic or corona wind) by a gas discharge across two electrodes without the need for moving parts. Basically, EHD flows occur when a high voltage is applied between a highly curved corona electrode (the emitter electrode) and a grounded surface (the collecting electrode), creating an electric field gradient in the air gap between them. When a sufficient electric field is created at the corona electrode, the surrounding air molecules are ionized. The resultant charged ions are then accelerated under the effect of electrostatic forces towards the collector electrode, transferring their momentum and energy to the surrounding neutral air particles via collisions and inducing air movement known as an ionic wind.

A number of studies have explored purely EHD driven airflows for convective heat transfer (for example, [10-14]) after the earliest work presented by Marco and Velkoff in 1963 [15], while the majority of the reported investigations have focused on using EHD as secondary air generators to mix airflows for boundary layer modification and heat transfer enhancements [16-19]. However, it is only recently that the application of purely EHD technology has received increasing attention as an attractive alternative to rotary fans for localized cooling of microelectronic components [20, 21] or in integration with heat sinks [22-24]. The first practical and successful integration of EHD air movers into a real-world electronic application has been performed by Jewell-Larsen et al. in 2009 [25]. In their work, an EHD blower of a wire-to-plate configuration was installed instead of a mechanical fan in a retrofitted laptop, with grounded plates acting as the microelectronic chip heat sink. Results of an un-optimized EHD device revealed promising cooling performance with lower installation size and acoustic level, compared to the rotary fan.

One of first studies to examine the possibility of employing electrostatic blowers for practical use was reported in the early 1960's by Robinson [26], using a needle-to-ring electrode configuration to generate electric wind in a tube. The author concluded that despite the low conversion efficiency (less than 1%) achieved in his geometric design, he explicitly mentioned that electrostatic blowers have attractive advantages over conventional mechanical fans, and recommended that more research on improving conversion efficiency of EHD pumps is required.

Although the attempts to develop corona wind generation were made early, the most interesting investigations have been conducted over the last decade [27-29]. Based on performance of airflow generation, few studies have been performed to optimize the design geometry of EHD blowers in the absence of external bulk flow and without any integration between the collector electrode and heat exchange surface.

Kalman et al. [30] were the first to investigate experimentally the optimization of an electrostatic blower and explore its potential as a cooling system for electronic components. The EHD device consisted of a positively charged wire electrode, 0.5 mm in diameter, stretched between two collecting inclined wings located over a heated horizontal plate. The design parameters, including the gap between collecting wings, the vertical electrode gap, and the wing inclination angle, were optimized based on the highest achieved airflow production and heat transfer rate. The results showed that the optimized EHD blower was able to increase the heat transfer by more than double compared to free convection. This study was later extended by Rashkovan et al. [31] by reducing the emitter wire diameter to 0.2 mm in order to enhance the electric field strength, aiming to develop the EHD air blower and improve its performance. Based on the highest heat transfer coefficient achieved, the optimum configuration was obtained by using a corona wire located between two parallel collecting wings, where the wire is collinear with the adjacent ends of the collecting plate wings, creating an angle of 55.5^{o} with their far ends. The new optimized design was able to increase the heat transfer coefficient by up to 3 times higher than the free convection, resulting in a 50% increase in heat transfer over that obtained by the EHD blower presented in the previous study. However, no information regarding the conversion efficiency values or the EHD operating power was included in these studies.

Komeili et al. [32] experimentally demonstrated the application of a miniature EHD blower by investigating the flow characteristics of a wire-to-rod EHD pump operated in a circular duct using ranges of negative applied voltage (up to −20 kV), grounded rod diameter (1.5–3.1 mm), duct diameter (6.5–20 mm), and electrode gap to duct dimeter ratio (0.63–1.16). Experiments showed that the EHD pump was capable of producing a maximum airflow rate of 40 l/min at −16 kV, using a pipe diameter of 20 mm with about 0.35 W input power. Another study was conducted later by Takeuchi and Yasuoka [33] using similar electrode configuration to investigate the EHD pump efficiency under negative corona discharge. Results showed that the EHD pump was more efficient by two times based on flow rate generation compared with a conventional rotary fan of equivalent diameter under the same operating conditions.

Moreau et al. [34] presented an experimental study to optimize the mechanical characteristics of the ionic wind induced by a needle emitter through a tube. In their investigation, they considered the effect of voltage polarity and collecting electrode geometry (grid and ring configurations) as well as electrode gap and tube diameter. Results of the optimal configuration showed considerable performance with a maximum wind velocity and a flow rate up to 8 m/s and 0.4 l/s, respectively, with a conversion efficiency of 1.72%, using approximately 12 kV.

Although design optimization represents a critical factor to determine the performance and efficiency of EHD devices for practical implementation, where the thermal management requirements are inherently considered, optimization of miniature EHD air blowers based on the efficient levels of operating voltage and power has not been investigated. In this paper, a two-dimensional numerical model of a wire-to-plane EHD channel configuration is developed and validated carefully using COMSOL Multiphysics package against a range of experimental and numerical data. A numerical investigation and analysis are devoted to explore the influence of the main design parameters that affect the EHD flow characteristics, including the location and length of the collector electrode for a range of blower heights (up to 10 mm). The main purpose of the present study is to optimize the configuration of different miniature EHD air blowers based on pumping efficiency, key design factors and practical implementation requirements.

II. NUMERICAL MODELING

A. EHD Governing Equations

The EHD flow induced by corona discharge is described by the following equations. The electric field intensity, $\vec{E}$, and the electric potential, V, are defined by Poisson's equation as,

$$\vec{\nabla} \cdot \vec{E} = \nabla^2 V = -\frac{q}{\varepsilon_0} \tag{1}$$

where q is the space charge density (C/m^3) and ε_0 is permittivity of free space (= 8.854×10^{-12} C/V.m). The charge transport equation that couples the electrostatic and Navier-Stokes equations for the airflow is derived by combining the following three equations:

i. The electric current density equation,

$$\vec{J} = \mu_p \vec{E} q + \vec{U} q - D\vec{\nabla} q \tag{2}$$

where μ_p is the air ion mobility in the electric field (m^2/V.s), $\vec{U}$ is the velocity vector of airflow, and D is the diffusivity coefficient of ions (m^2/s). The three terms on the right side of equation (2) represent the charge conduction (the ion movement due to the electric field), charge convection (transport of charges by the airflow), and charge diffusion, respectively [35].

ii. The continuity equation for electric current,

$$\vec{\nabla} . \vec{J} = 0 \tag{3}$$

iii. The conservation of mass equation,

$$\vec{\nabla} . \vec{U} = 0 \tag{4}$$

Combining equations (2) and (3) and using the continuity equation (4) gives the charge transport equation,

$$\vec{\nabla} . (\mu_p \vec{E} q - D\vec{\nabla} q) + \vec{U} . \vec{\nabla} q = 0 \tag{5}$$

Since the value of the air velocity ($\vec{U}$), which represents the charge convection term in equation (5), is very small compared with the drift velocity of ions ($\mu_p \vec{E}$) in the charge conduction term, it can be neglected [36]. The Navier-Stokes equations and continuity equation (4) describe the fluid dynamic part of the model for steady state incompressible airflow under the effect of the electrostatic force,

$$\rho \vec{U} . \vec{\nabla} \vec{U} = -\vec{\nabla} p + \mu \nabla^2 \vec{U} + q\vec{E} \tag{6}$$

where ρ is the air density (kg/m^3), p is the air pressure (Pa), μ is the air dynamic viscosity (Ns/m^2), and the term of $q\vec{E}$ represents the body or Coulomb force (N/m^3).

B. Space Charge Generation

The air gap across the corona and collecting electrodes can be divided into ionization and drifting regions. The space charge density in the ionization zone can be neglected as it contains a mix of electrons and positive ions at similar magnitudes, compared to the drift zone, which contains ions of a single polarity and neutral air molecules [35]. Using Peek's empirical formula [37], the electric field strength E_e created on a smooth surface of a positively charged wire electrode at standard air conditions can be estimated by,

$$E_e = E_0 (1 + (0.0262 / \sqrt{R_e}) \tag{7}$$

where R_e is the corona wire radius (m), and E_0 is the breakdown electric strength of air (3.23×10^6 V/m).

III. VALIDATION OF THE NUMERICAL METHOD

A. Solution Domain and Boundary Conditions

The experimental data and numerical results of a wire-to-plane EHD channel presented in [38] were used to validate the accuracy of the numerical simulation method performed in this paper. The EHD channel geometry consists of a fine wire electrode, 25 μm in diameter, stretched horizontally between and parallel to two dielectric plates, forming the channel walls. The channel width, w, (or the distance between the dielectric channel sidewalls) is 100 mm. Two conductive and grounded stripes of 0.1 mm thickness are positioned at the top and bottom of the channel walls and located downstream of the wire electrode at a distance equal to the channel height, h. A cross-section of the EHD channel geometry used in the validation simulation is shown in Figure 1.

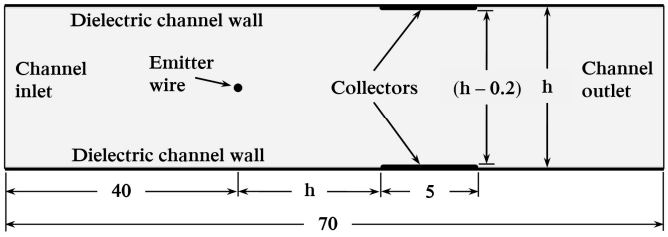

Fig. 1. Cross-section of the EHD channel geometry [38] used in the numerical validation. Dimensions in millimeters.

In order to save the solution computation time, a symmetry boundary condition is applied at the horizontal plane centered between the channel walls of the simulation domain. The coupled equations of the electric field (1), the charge transport (5), and the airflow (4 and 6), are solved in the half domain using the commercial package, COMSOL Multiphysics (V5.1), a partial differential equations (PDEs) solver based on the finite element method, using the modelling parameters listed in Table I. The following main modules were used and coupled to represent the governing equations of EHD flow in COMSOL Multiphysics,

i. The electrostatics module, which is used to solve Poisson's

equation for the electric and potential fields (1).

ii. A partial differential equation is created to represent the charge transport equation (5).

iii. The laminar flow module, which is used to solve the fluid dynamic equations (4) and (6) for a steady incompressible flow under the effect of volume force.

TABLE I
GEOMETRIC PARAMETERS [38] AND NUMERICAL MODELLING VALUES USED IN THE PRESENT VALIDATION MODEL

Parameter	Value
Positive applied potential, V_e	0 – 10 kV
Ion mobility coefficient, μ_p	2.1×10^{-4} m^2/V.s
Charge diffusion coefficient, D	5.3×10^{-5} m^2/s
Density of air, ρ	1.23 kg/m3
Dynamic viscosity of air, μ	1.8×10^{-5} N.s/m^2
Corona wire radius, R_e	0.0125 mm
Channel height, h	2 , 6 mm
Channel length, L	70 mm
Channel width, w (= corona wire length)	100 mm
Horizontal distance between the electrodes, (= h)	2 , 6 mm
Collecting surface length	5 mm

The electrostatic mode is modeled by applying a positive potential to the emitter wire surface, while the collecting surface at the channel wall is grounded. For charge transport, a zero diffusive flux condition (Neumann condition) is imposed on all boundaries excluding the surface of the corona wire, where a space charge surface density under an iterated Dirichlet condition is applied. This is based on the fact that the diffusion term is very small compared to the conduction term in equation (5), so that its effect on charge density can be neglected [36, 39]. For the flow equations, a standard hydrodynamic boundary condition of no-slip is applied to all solid surfaces of corona electrode and channel wall. An outlet-flow condition and zero pressure is applied at the channel outlet, while a normal flow (v = 0) with a horizontal velocity component, u, prescribed from Bernoulli's equation is used at the channel inlet [35, 38, 40, 41]. More details can be found in [38, 42]. The boundary conditions for the space charge density can be obtained by applying Kaptsov's assumption at the external surface of the ionization zone, which suggests that the electric field increases proportionally to the applied voltage below the corona onset level, but will preserve its value after the corona is initiated [43]. Under this assumption, the space charge resulting from corona discharge can be estimated by assuming that the electric field strength created at the surface of the corona wire due to the applied voltage is equal to that obtained from Peek's equation (7). The solution procedure of the numerical simulation method is shown in Figure 2.

A mesh independence study was performed for the half domains of 2 and 6 mm channel thicknesses with increased mesh refinements in the vicinity of the corona electrode, where gradients in the charge density and electric field are the highest. The numerical modelling equations were solved on three levels of mesh density generated with (62230, 98464 and 151800 triangular elements) for h = 2 mm, and (34115, 53500 and 81075 elements), for channel height of 6 mm. Results showed that the maximum discrepancy in average air velocity was approximately 0.15% between the last two mesh densities of each domain height, and therefore the second density levels were adopted. The same procedure of the mesh independence test was followed for the other domain heights considered in this study (h = 4, 8 and 10 mm). Figure 3 shows the mesh distribution and refinement on both electrodes for a half solution domain of h = 6 mm.

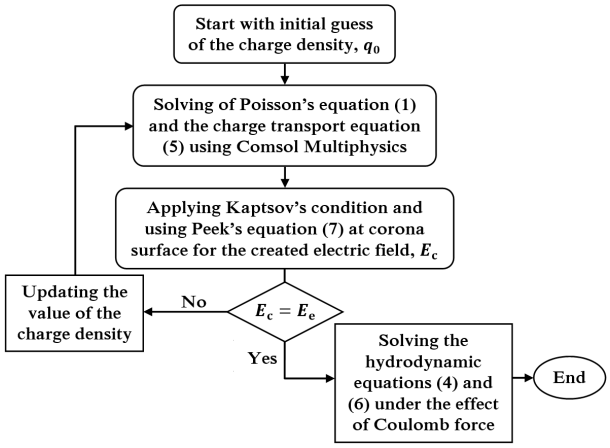

Fig. 2. Numerical solution procedure of the present modelling.

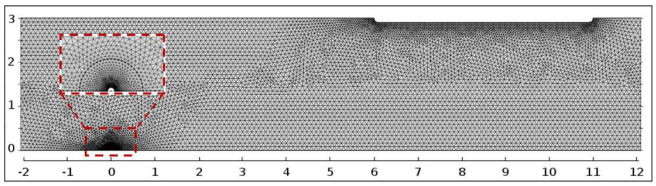

Fig. 3. Distribution of mesh element density for a half computational domain of the EHD blower geometry with h = 6 mm using approximately 53,000 triangular elements. The semicircle around the corona wire was used to define mesh refinement. Dimensions in millimeters.

B. Numerical Validation Results

The results of numerical solution for the EHD flow induced through ducts of 2 and 6 mm thicknesses at 15 W/m are illustrated in Figure 4. The plots show the distributions of the electric potential with the electric field lines (top panel), the charge density with the body force across the electrodes (center panel), and the generated air velocity of ionic wind through the channel (bottom panel). Further validation results are shown in Figure 5, which compare the airflow rates and the static pressures of the present simulation against experimental data and numerical results presented in [38], for a range of input power. The electrostatic pressure created due to the body force, which acts on the collecting surface and equals the channel static pressure, can be calculated by integrating the body force within the volume across the electrodes [38, 44],

$$\Delta P = \int_{vol} F \, \mathrm{d}v = \int_{vol} qE \, \mathrm{d}v \qquad (8)$$

where q and E are the charge density and the electric field strength within the electrode gap, respectively. The figure shows good agreement between the numerical results though

relatively acceptable differences can be seen compared to the experimental data. As explained in [38], the noticeable deviation between the simulated and measured pressure values for the 2 mm channel thickness was due to emitter wire misalignment in the experiments. This benchmark demonstrates the accuracy of the present numerical approach performed using COMSOL Multiphysics.

IV. Results and Discussion

A. Numerical Configuration Domain

The EHD channel geometry used for the present numerical study is shown in Figure 6. It is similar to that used in the validation model but with neglecting the collecting stripe thickness and increasing its length, *b*, to 10 mm, whereas the channel length is reduced by 20 mm. The same modelling parameters used in the validation model are adopted, including the corona wire diameter, which is recommended in compact EHD blowers to create a strong electric field using low levels of operating voltage [31, 42]. The numerical analysis is established to explore the impact of several design parameters on the EHD air blower efficiency and optimize its geometry based on ranges of fixed powers and applied positive voltages. These parameters include the collector location from the emitter electrode and the collecting surface length at the channel walls for a range of blower heights, as listed in Table II. In the present 2D simulation, it is assumed that the EHD blowers are wide enough with negligible sidewall effects on the flow characteristics.

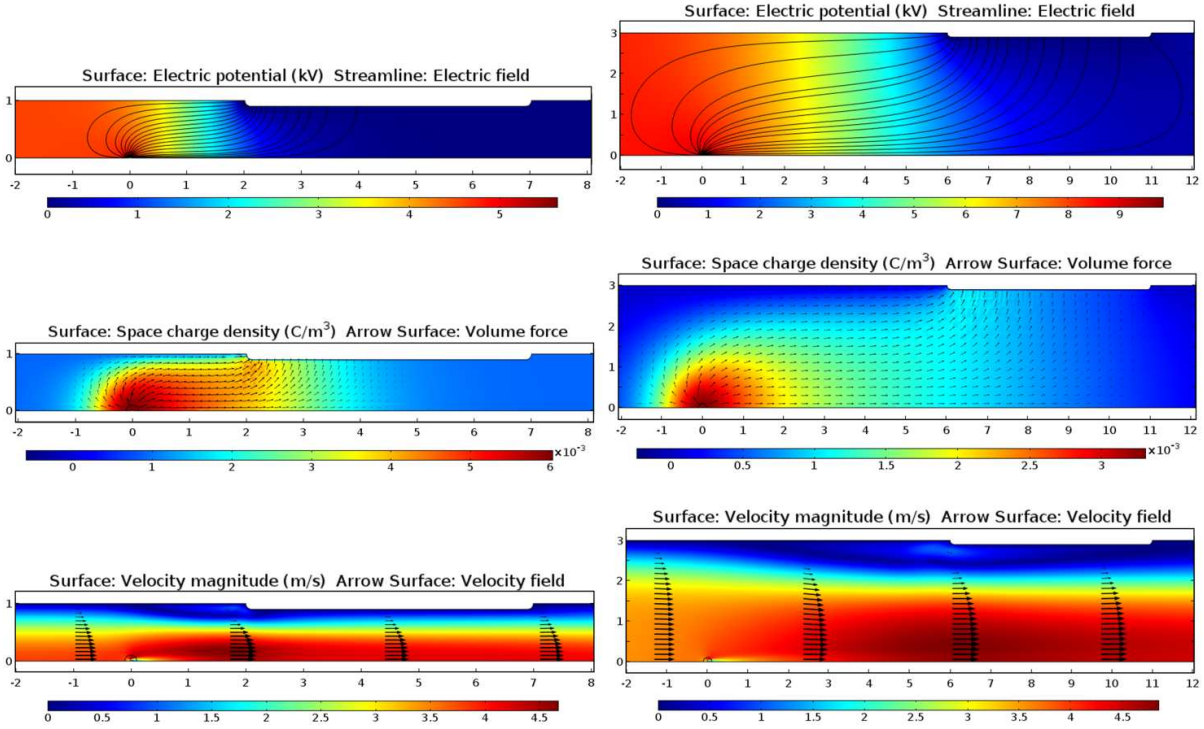

Fig. 4. Numerical validation results as surface map distributions of a half of the duct geometry generated at 15 W/m for h = 2 mm (left column) and h = 6 mm (right column), showing: (at top) electric potential with electric field lines, (at center) space charge density with coulomb force distribution as arrows, and (at bottom) air velocity distribution. Dimensions in millimeters.

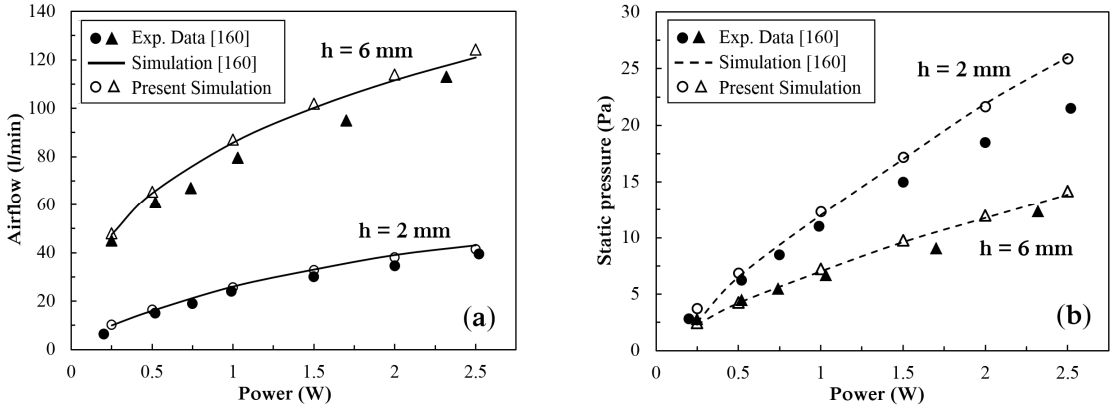

Fig. 5. Comparison of experimental and numerical results of EHD air blowers with h = 2 and 6 mm and w = 100 mm, showing the operating power as a function of (a) airflow rate, and (b) static pressure.

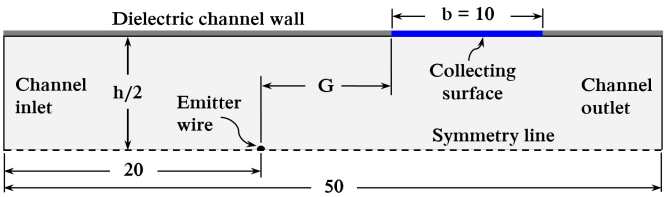

Fig. 6. Half domain of the EHD blower geometry used in the present numerical study. Dimensions in millimeters.

TABLE II
GEOMETRIC AND MODELLING PARAMETERS OF THE PRESENT STUDY

Parameter	Value
Overall range of applied potential, V_e	2 – 17 kV (Positive)
Corona wire diameter, d	0.025 mm
Channel length	50 mm
Channel height, h	2 – 10 mm (in 2 mm steps)
Horizontal gap between electrodes, G	0 – 7 mm
Collecting surface length, b	3 – 17 mm

B. Optimization of the Collector Location

In this section, the prediction of the optimal collector location relative to the emitter electrode, which is defined by the horizontal electrode gap G, and its influence on the EHD air blower performance are discussed. The electrode gap was changed from G = 0 to 7 mm (in 1 mm steps), whereas the blower height, h, was varied by five levels from 2 to 10 mm.

It is important to bear in mind that the wire-to-plane EHD channel of a rectangular cross-section area is the most preferred geometry proposed to be integrated as an EHD cooling system in thin electronic applications such as laptops, where the flexibility to control the blower thickness and width is required. In addition, the range of blower heights considered in this study lies within the thickness of current miniaturized and highly demanded consumer devices, where the performance of rotary fan degrades as the device dimensions reduce. Therefore, when the miniature EHD blowers are applied for practical devices as cooling systems, both the operating power and the level of applied voltage represent critical factors in thermal management considerations due to their impact on the produced airflow rate and the possibility of implementation. In small form factor electronic applications, a compact high voltage multiplier (usually on the order of kilovolts) must be integrated as a part of the EHD system in order to initiate and sustain the corona discharge process and generate EHD flow. The design of miniaturized, efficient and low cost high voltage multipliers represents one of the integration and practical challenges [25]. From a design perspective, reducing the value of operating voltage to the efficient level in compact applications is a needed feature, and a delicate balance for improving the flow generation must be made carefully. Therefore, the design optimization of the EHD blower geometry will be performed based on pumping performance by fixing the operating power and the applied voltage at the corona wire for a range of blower thickness in order to predict the optimal and the most effective locations of the collecting surface.

1) The Case of Constant Input Power: For a range of fixed input power from 5 to 25 W/m (calculated per wire length), Figure 7 illustrates how the collector location of different blower heights affects the outlet mean velocity and the applied voltage that corresponds to each level of input power. It can be seen that, for each height, both the ionic wind velocity and the applied voltage required to preserve the input power at a fixed level increase as the consumed power and the gap G increase. The figure also shows how the blower height (or the vertical electrode gap) affects the magnitude of outlet velocity, as will be discussed later. In fact, the increase in the horizontal gap and the associated potential improves the distribution and directions of the enhanced electric field lines along the grounded surface, adding relatively higher kinetic energy to the horizontal components of the Coulomb force, which have the main impact of moving the ionic wind towards the channel outlet. However, the trends show that the increase in the air velocity becomes slight after certain locations, regardless of the value of applied voltage, and can be neglected after G = 5 mm for all given levels of heights and input powers. Indeed, further increases in the electrode gap at a fixed operating power cause a decrease in the effective angle of the drifting region between the emitter and the collecting surface, leading to an increase in the applied voltage required and resulting in a modest enhancement in the ionic wind velocity.

In order to reduce the level of the applied voltage and determine the most effective location of the collecting surface for each height, the percentage increase of both the average air velocity and the applied potential was calculated for shorter steps of G and two levels of input power (the lowest and highest levels considered in this study), as shown in Figure 8. It can be observed that the percentage increase in the air velocity at the first step (G = 0.5 mm) over that generated at the location of G = 0, is higher than that of the required applied potential for all blower heights. However, the augmentation in the velocity tends to decrease with increasing G, compared to that of the potential, which (the latter) reaches its peak level at certain locations before it tends to drop. It was found that when the increase in the potential reaches its peak, the percentage increase in the air production accounts for approximately 50% of that in the applied voltage, and all increases in the voltage beyond these gaps are relatively inefficient in improving the air velocity. Table III summarizes the total percentage increase in both the produced air velocity and the required applied voltage calculated at the predicted optimal locations over that at the initial location (G = 0), for two fixed levels of operating power. It can be seen that the increase in the required voltage is associated with approximately an equivalent improvement in the air velocity. However, further increase in the electrode gap beyond the optimal locations does not lead to efficient balance in both terms. For example, although moving the collecting surface by 0.5 mm beyond the proposed optimal location in the blower of h = 2 mm improves the air velocity by approximately 6–8%, a significant relative increase in the applied voltage by more than 20% is required. Moreover, for the thicker blowers, increasing G by 0.5 mm leads to modest increases in the velocity by only 3% or less, regardless of the increases in the associated applied voltages, which are still higher (typically 3 times higher) compared to the corresponding velocity increases.

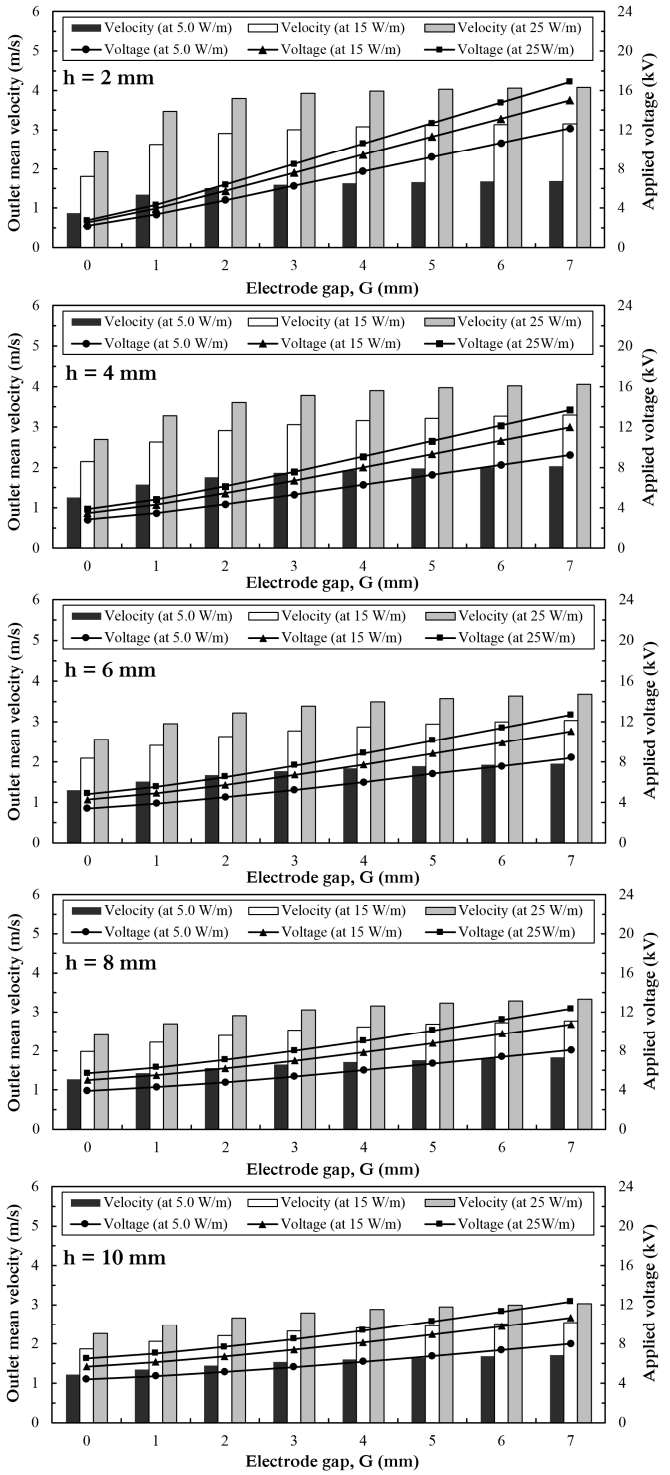

Fig. 7. Variation of average air velocity and applied potential with the horizontal electrode gap, G, for different blowers and a range of fixed input power.

Therefore, the locations, which are indicated by arrows in Figure 8, can be considered as the optimal and the most effective gaps for the case of constant input power, and given by the following formula,

$$G_{\mathrm{p}} = (h / 4) + 0.5 \qquad (9)$$

where G_{P} is the optimal electrode gap (mm), for the case of constant input power, and h is the blower height (from 2 to 10 mm).

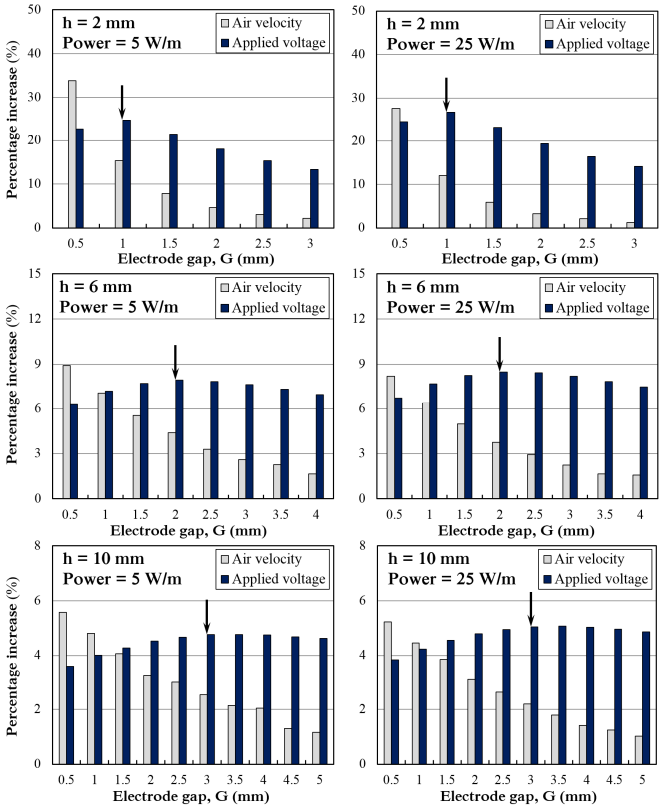

Fig. 8. Electrode gap as a function of the percentage increase (each calculated over that of the former step of G) in both average air velocity and applied potential for different blowers at fixed input powers (5 W/m for left column and 25 W/m for right column). Figures for h = 4 and 8 mm are not shown.

TABLE III
TOTAL PERCENTAGE INCREASE IN THE AVERAGE VELOCITY AND APPLIED VOLTAGE CALCULATED AT THE OPTIMAL LOCATIONS OF DIFFERENT BLOWERS FOR TWO LEVELS OF FIXED OPERATING POWER

Blower height, h (mm)	Optimal electrode gap, G (mm)	Operating Power (W/m)	Total percentage increase over that at the initial location (G = 0)		Percentage increase calculated at one step (0.5 mm) beyond the optimal locations	
			Velocity (%)	Voltage (%)	Velocity (%)	Voltage (%)
2	**1**	5	**49**	**47.5**	7.8	21.5
		25	**40**	**51**	5.9	23
4	**1.5**	5	**30.6**	**33.3**	4.8	11.6
		25	**26.2**	**36**	4	12.5
6	**2**	5	**26**	**29**	3.1	7.9
		25	**23.3**	**31**	2.9	8.4
8	**2.5**	5	**24.2**	**27.2**	2.5	6
		25	**22**	**28.8**	2.3	6.3
10	**3**	5	**23.2**	**25.7**	2.1	4.8
		25	**21.5**	**27.4**	1.8	5.1

2) The Case of Constant Applied Voltage: In order to optimize the EHD blower geometry at a constant applied potential, an appropriate range of three operating voltages (increased by 1 kV) were applied for each blower height. Each range of applied voltage was chosen to be close to that required to fix the operating power (from 5 to 25 W/m) used

in the previous optimization method. In this case, the optimal locations of the collector for each height can be estimated based on the EHD blower performance for a given range of operating voltage. Therefore, the electro-mechanical (or transduction) efficiency, which is the percentage of electrical power converted into mechanical (kinetic) power, is adopted [34]. The produced mechanical power P_m (calculated per channel width) can be expressed as,

$$P_m = Q\,\Delta P = \frac{1}{2}\,\rho\, h\, U_{av}^{3} \tag{10}$$

where Q is the flow rate per width (m^2/s), ΔP is the dynamic pressure rise (Pa), ρ is the air density (kg/m^3), U_{av} is average air velocity at the channel outlet (m/s), and h is the channel height (m). The electrical power P_{elec} can be calculated from,

$$P_{elec} = I_c\, V_e \tag{11}$$

where V_e is the applied potential (V), and I_c is the corona current calculated per channel width (or the wire length) (A/m). Thus, the electro-mechanical efficiency, η, of the EHD blower is given by,

$$\eta = \frac{P_m}{P_{elec}} \tag{12}$$

Figure 9 shows that the efficiency of each blower grows with increasing the horizontal gap, G, reaching its maximum value at a certain location before it tends to drop or maintain its value at the low applied voltage, or show a slight increase at a higher potential as the blower becomes thicker. As mentioned in the previous section, moving the collector electrode towards the outlet direction can enhance the distribution of the electric field lines and improve the kinetic energy imparted to the flow by the horizontal components of the Coulomb force. However, further increase in the gap at a given applied potential decreases the impact of the electric field, especially for the thin channels, due to the reduction in the effective collector area. In addition, the trends reveal that the blower efficiency increases as the blower height increases for all applied voltages, reaching its highest values at the highest applied voltages. Indeed, as the duct becomes thicker and the applied voltage increases, the electric field lines across the electrodes can be strong enough with a wider effective drifting angle to reach a larger area of the collecting surface, compared to the thinner ducts, leading relatively to a better ionic wind generation. Therefore, the locations that show the highest EHD blower's efficiency for the range of applied voltage, which are identified in Figure 9 by dashed lines, can be considered as the optimal gaps, although modest increases in the efficiency can be observed beyond them at the highest applied voltage. These locations can be simply given by the following formula,

$$G_V = (h/2) - 0.5 \tag{13}$$

where G_V is the optimal electrode gap (mm), at a constant applied voltage, and h is the blower thickness (from 2 to 10 mm). It is useful to state that the difference in the optimal collector locations in both cases is mainly attributed to the optimization method used in each case. In the first method, the level of input power is fixed whereas the ion current decreases and the applied voltage increases with the electrode gap. In contrast, the second method has fixed applied voltages, whereas the ion current and thereby the consumed power decrease with increasing the electrode gap. Therefore, when the application in the practical implementation is mainly controlled by a limited range of operating power, regardless of the level of applied voltage, the selection of the first optimization method is recommended, whereas the second method offers the best predicted efficiency of the EHD device when its operating voltage is limited.

C. Optimization of the Collector Length

In the previous section, the optimal locations of the collecting surface were estimated with a fixed length of b = 10 mm. However, the effective collector length is not equal for all presented cases but depends on its location (the horizontal electrode gap), the blower height (the vertical electrode gap), and the level of applied potential (the electric field strength). Therefore, the effective collector length can be determined at its optimal location for each blower thickness, based on both cases of operating method. The highest values of the power and applied potential used in each optimization case were adopted in order to create the strongest electric field across the electrodes, and also to ensure the validity for lower operating levels. Figure 10 shows the influence of the collector length on the ion current created at a fixed input power at 25 W/m (generated by a range of corresponding voltages from 4.3 to 8.5 kV), and a fixed applied voltage (in a range from 5.5 to 7.5 kV), for different blower heights. It can be observed that the effective collector length increases as the blower becomes thicker for both cases of operating method. For example, the collector length required for the blower of h = 2 mm at a fixed power is 3 mm, and there is no effect on the corona current beyond this length, whereas the blower of h = 10 mm requires a collector with at least 15 mm length before being independent of the created current. This behavior is due to the change in the effective drifting angle of charged ions across the electrodes, which expands as the blower height (or the vertical electrode gap) increases, as shown in Figure 11. The trends also reveal that the maximum effective length of the collector electrode for each blower differs depending on the method of applying voltage. Indeed, this change is due to the difference in the level of applied voltage and the optimal collector location defined by equations (9) and (13).

The predicted results indicate that extending the collector electrode over certain lengths does not have any impact on the ion current and the generated ionic wind, within the overall range of operating voltage used in the present investigation.

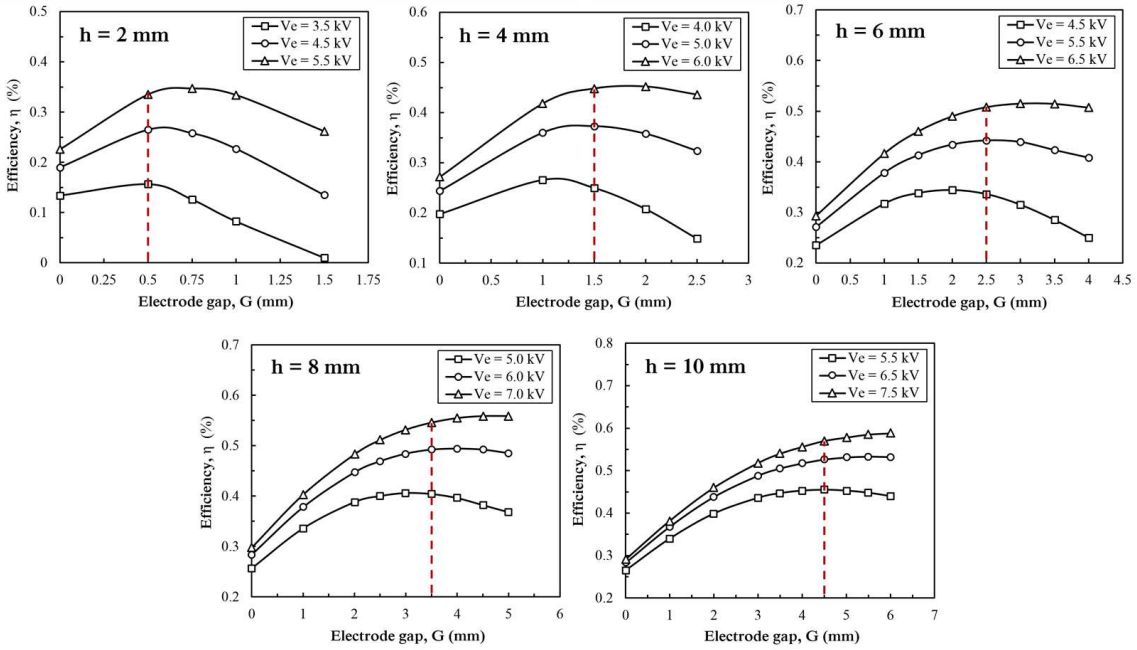

Fig. 9. Electrode gap as a function of the electro-mechanical efficiency for different blowers at fixed applied voltages.

The dashed lines in Figure 10 indicate the maximum effective lengths required for each optimized blower based on each case of optimization method, and can be defined by the following expressions,

$$b_P = 1.5\,h \tag{14}$$

$$b_V = h + 2 \tag{15}$$

where b_P and b_V are the maximum effective lengths (each in mm) for the cases of constant power and applied voltage, respectively, and h is the blower thickness (2 – 10 mm). From a design perspective, reducing the collector to its effective length in the thin EHD blowers offers further miniaturization in size, which is a required merit in space constrained applications. In addition, using the whole effective length of the collecting surface in the thicker EHD pumps can enhance the heat removal from the channel walls when the heated surface is used as a collector in some cooled applications. Figure 12 illustrates and summarizes the optimal electrode gaps, G, and the maximum effective lengths, b, of the collector electrode predicted using the two operating methods for the range of blower heights considered in this study.

It is useful to state that the predicted optimal design parameters from equations (9), (13), (14), and (15) are only valid for the wire-to-plane EHD channel configuration using the corona wire diameter adopted in this study within the ranges of blower heights and levels of operating conditions. However, using thicker corona wires of diameters larger than 25 μm will decrease the electric field strength created across the electrodes and the resultant airflow. In this case, these equations can be used as a reference to determine the maximum electrode gaps and collector lengths for the given range of blower heights. Moreover, using thicker emitter wires leads to lower efficiency and a significant increase in the voltage required to generate certain flow rates in miniature EHD blower [42], which is practically undesirable from a design perspective. On the other hand, although using finer corona wire is possible but more complex in practical integration, the presented equations here can also be used as a useful baseline to predict the optimal design parameters using the same EHD geometry, which are expected to be higher in values due to the stronger electric field created.

Regarding the application of the investigated blowers based on the considered range of heights, the thicker optimized EHD blowers (h = 6 – 10 mm) can be used in small-scale and thin consumer devices such as laptops to cool heat sinks of equivalent thickness. Unlike conventional fans, the height of EHD blowers is independent of the length and width dimensions, offering an attractive flexibility to shorten the length and extend the width as required. For the thinner optimized blowers (h = 2 – 4 mm), a set of multiple wires can be integrated as emitter electrodes with a grounded plate-fin heat sink and positioned at the predicted optimal locations to generate effective cooling airflow through the fin channels, even at low velocities. In this case, the wire diameter, the level of operating voltage and the power consumption are very critical and important factors to account in practical cooling solutions.

D. Influence of the blower height

Figure 13 shows the operating input power and the blower thickness as functions of the average air velocity generated by different optimized EHD blowers. The trends reveal that the air velocity produced by each blower increases with increasing power and decreasing blower height. When the power

increases at a given electrode gap, the impact of the electric field and the electrostatic forces becomes stronger to impart higher kinetic energy into the flow, leading to an enhanced ionic wind generation, as shown in Figure 13a. However, at a given fixed power, the ionic wind production decreases as the blower becomes thicker, although both the required potential and the optimal location steps of the collector towards the outlet direction increase with the height (Figure 13b). Indeed, the increase in the blower height or the vertical distance between the electrodes leads to an increase in the vertical components of the Coulomb force, causing a reduction in the flow production towards the desirable direction. The blower of h = 2 mm shows different behavior at low input powers among other heights due to the short effective length of its collector.

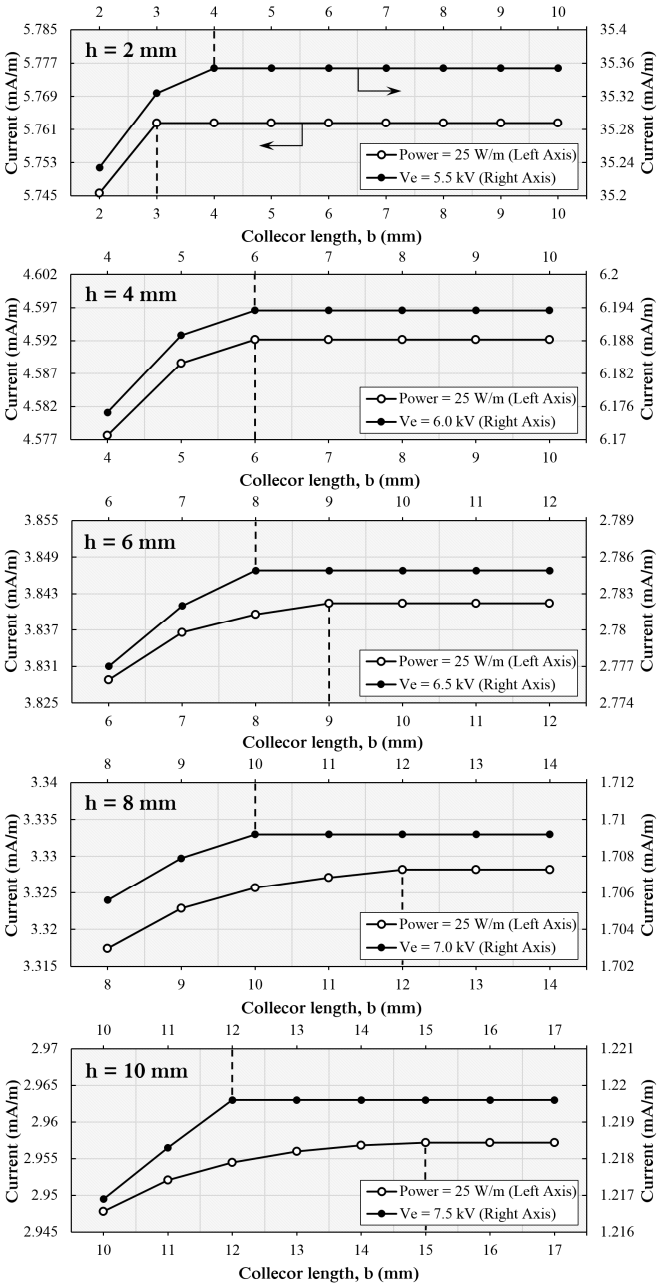

Fig. 10. Effect of collector length on the discharge current created by different optimized EHD blowers using two operating methods.

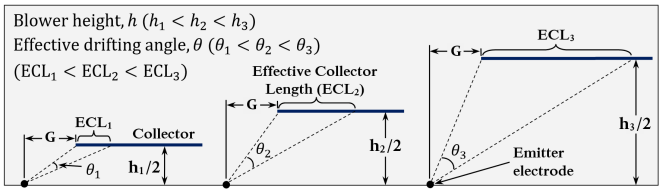

Fig. 11. Effect of blower height, h, on the effective drifting angle, θ, created between the emitter electrode and the effective collector length.

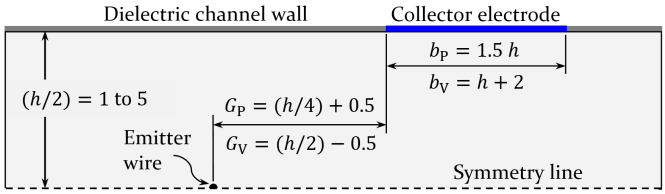

Fig. 12. The optimal electrode gaps, G, and the maximum effective lengths, b, of the collecting surfaces for the two cases of operating method. Dimensions in millimeters.

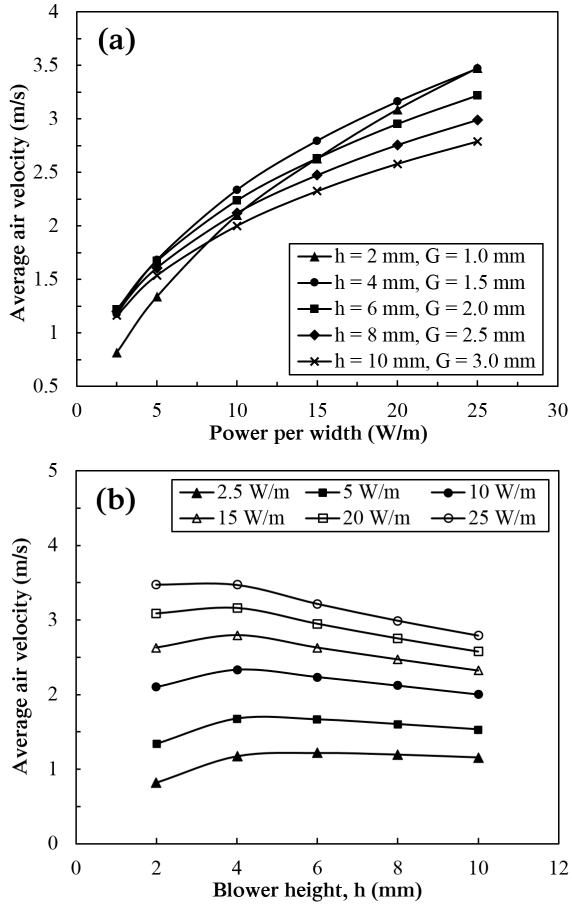

Fig. 13. Effect of (a) input power and (b) blower height, on outlet average air velocity.

E. Scaling laws for optimized EHD blowers

Airflow performance scaling laws for EHD blowers have been first investigated by Jewell-Larsen et al. [38]. Based on measured results and numerical modelling, they proved that EHD air movers can be considered as an ideal pressure source by neglecting the internal flow resistance of the EHD duct. Moreover, they presented scaling law relations as functions of

the width, thickness, and operating power of the device to predict airflow rates and static pressures of EHD air blowers. Results showed that the scaling laws of the EHD-driven flow devices can be expressed as follows,

$$\text{For the airflow rate, } Q \propto (Power)^{1/3}\ h^{2/3} \tag{16}$$

$$\text{For the static pressure, } \Delta P \propto \left(\frac{Power}{h}\right)^{2/3} \tag{17}$$

Following these scaling laws of the ideal EHD flow device, Figure 14 shows both the flow rate and static pressure as a function of the power density for a range of blower heights. The power density of each term can be calculated from equations (16) and (17), respectively, assuming that a constant transduction efficiency relates the mechanical (10) and electric (11) powers [38], with including the blower width, *w*, in (10). The predicted results of flow rate and static pressure of various optimized blowers show good agreement with those expected from the scaling laws as the data of all heights falls linearly into a straight line. This indicates that the proposed optimal collector location of each blower height of the present configuration is valid to provide an airflow performance that lies within the scaling laws of ideal EHD flow devices.

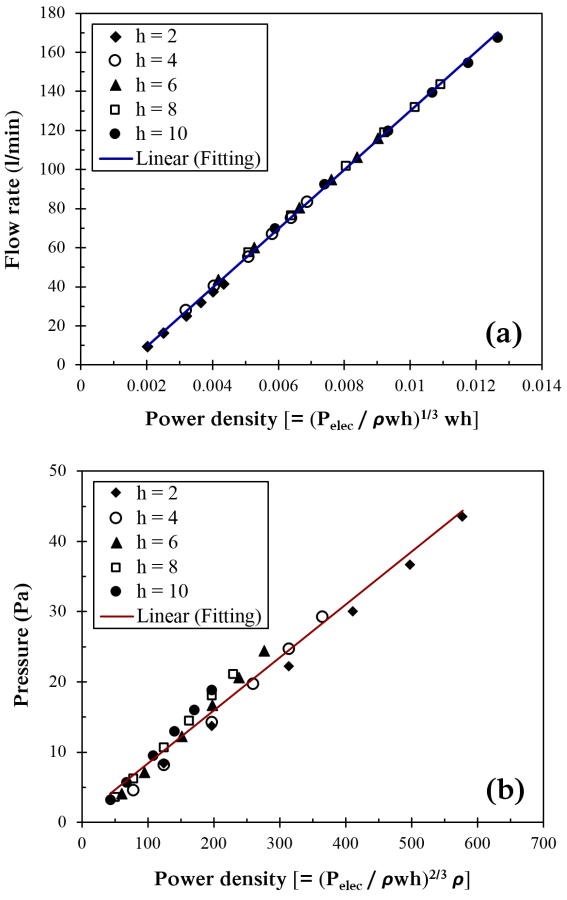

Fig. 14. Power density related to the scaling laws of ideal EHD devices as a function of (a) flow rate and (b) static pressure, for different optimized blowers.

V. Conclusions

A numerical analysis and optimization of miniature EHD air blowers are performed based on an accurate numerical approach validated successfully against previous data. The investigation is devoted to explore the influence of the main design parameters that affect the EHD flow characteristics, including the location and length of the collecting electrode for different levels of the EHD blower height in a range from 2 to 10 mm. By fixing both the input power and the applied voltage, the horizontal electrode gap and the most effective collector length for each blower height are optimized and defined by simple expressions. Although the predicted optimized wire-to-plane EHD channel configurations are valid only for the corona wire diameter adopted in this study, these optimal parameters can be used as a useful reference when thicker or finer corona wires are used for the given ranges of blower heights and operating conditions. Results of produced flow rates and static pressures obtained by the optimized blowers are found to agree well with those predicted by the previously reported EHD scaling laws of ideal EHD flow devices. Future work will include the effect of blower sidewalls on EHD flow characteristics using three-dimensional modeling, and the potential of employing the optimized EHD configurations in integration with thermal-exchange structure such as heat-sink channels.

Acknowledgment

Funding support from the Higher Committee for Education Development in Iraq (HCED) is gratefully acknowledged. The authors would like to thank Dr. Gregory de Boer for his appreciated help in using COMSOL.

References

1. Wang, H.-C., N.E. Jewell-Larsen, and A.V. Mamishev, *Thermal management of microelectronics with electrostatic fluid accelerators.* Applied Thermal Engineering, 2013. **51**(1): p. 190-211.
2. Rodgers, P., V. Eveloy, and M.G. Pecht. *Limits of air-cooling: Status and challenges*. in *Semiconductor Thermal Measurement and Management Symposium, 2005 IEEE Twenty First Annual IEEE*. 2005. IEEE.
3. Walsh, E., P. Walsh, J. Punch, and R. Grimes, *Acoustic emissions from active cooling solutions for portable devices.* IEEE Transactions on Components and Packaging Technologies, 2009. **32**(4): p. 776-783.
4. Grimes, R., P. Walsh, E. Walsh, and V. Egan. *The Effects of Diameter and Rotational Speed on the Aerodynamic Performance of Low Profile Miniature Radial Flow Fans*. in *ASME 2007 5th International Conference on Nanochannels, Microchannels, and Minichannels*. 2007. American Society of Mechanical Engineers.
5. Quin, D., *Micro scale axial flow fans.* Stokes Research Institute, Dept. of Mechanical and Aeronautical Engineering, PhD, University of Limerick, Limerick, Ireland, 2006.
6. Quin, D. and R. Grimes, *The effect of reynolds number on microaxial flow fan performance.* Journal of Fluids Engineering, 2008. **130**(10): p. 101101.
7. Day, S.W., P.P. Lemire, R.D. Flack, and J.C. McDaniel. *Effect of Reynolds Number on Performance of a Small Centrifugal Pump*. in *ASME/JSME 2003 4th Joint Fluids Summer Engineering Conference*. 2003. American Society of Mechanical Engineers.
8. Hanly, K., R. Grimes, E. Walsh, B. Rodgers, and J. Punch. *The effect of Reynolds number on the aerodynamic performance of micro radial flow fans.* in *ASME 2005 Summer Heat Transfer Conference collocated with the ASME 2005 Pacific Rim Technical Conference and Exhibition on*

Integration and Packaging of MEMS, NEMS, and Electronic Systems. 2005. American Society of Mechanical Engineers.
9. Walsh, P., V. Egan, R. Grimes, and E. Walsh. *Scaling of Flow Characteristics and Power Consumption With Profile Height for Miniature Centrifugal Fans*. in *ASME 2007 5th International Conference on Nanochannels, Microchannels, and Minichannels*. 2007. American Society of Mechanical Engineers.
10. Yabe, A., Y. Mori, and K. Hijikata, *Heat transfer augmentation around a downward-facing flat plate by non-uniform electric fields.* HEAT TRANSFER, 1978. **1000**: p. 20.
11. Franke, M. and K. Hutson, *Effects of corona discharge on free-convection heat transfer inside a vertical hollow cylinder.* Journal of heat transfer, 1984. **106**(2): p. 346-351.
12. Franke, M. and L. Hogue, *Electrostatic cooling of a horizontal cylinder.* Journal of heat transfer, 1991. **113**(3): p. 544-548.
13. Owsenek, B. and J. Seyed-Yagoobi, *Theoretical and experimental study of electrohydrodynamic heat transfer enhancement through wire-plate corona discharge.* Journal of Heat Transfer, 1997. **119**(3): p. 604-610.
14. Yonggang, Y., H. Junping, A. Zhongliang, Y. Lanjun, and Z. Qiaogen, *Experimental studies of the enhanced heat transfer from a heating vertical flat plate by ionic wind.* Plasma Science and Technology, 2006. **8**(6): p. 697.
15. Marco, S. and H. Velkoff, *Effect of electrostatic fields on free-convection heat transfer from flat plates.* ASME Paper No. 63-HT-9, 1963.
16. Velkoff, H. and R. Godfrey, *Low-velocity heat transfer to a flat plate in the presence of a corona discharge in air.* Journal of Heat Transfer, 1979. **101**(1): p. 157-163.
17. Takimoto, A., Y. Tada, Y. Hayashi, and K. Yamada, *Convective heat-transfer enhancement by a corona discharge.* Heat Transfer-Japanese Research;(United States), 1991. **20**(1).
18. Shooshtari, A., M. Ohadi, and F.H. França. *Experimental and numerical analysis of electrohydrodynamic enhancement of heat transfer in air laminar channel flow*. in *Semiconductor Thermal Measurement and Management Symposium, 2003. Ninteenth Annual IEEE*. 2003. IEEE.
19. Go, D.B., R.A. Maturana, T.S. Fisher, and S.V. Garimella, *Enhancement of external forced convection by ionic wind.* International Journal of Heat and Mass Transfer, 2008. **51**(25): p. 6047-6053.
20. Go, D.B., R. Maturana, R.K. Mongia, S.V. Garimella, and T.S. Fisher. *Ionic Winds for Enhanced Cooling in Portable Platforms*. in *Electronics Packaging Technology Conference, 2008. EPTC 2008. 10th*. 2008. IEEE.
21. Hsu, C.-P., N.E. Jewell-Larsen, I.A. Krichtafovitch, and A.V. Mamishev, *Heat-transfer-enhancement measurement for microfabricated electrostatic fluid accelerators.* Journal of Microelectromechanical Systems, 2009. **18**(1): p. 111-118.
22. Schlitz, D. and V. Singhal. *An electro-aerodynamic solid-state fan and cooling system*. in *Semiconductor Thermal Measurement and Management Symposium, 2008. Semi-Therm 2008. Twenty-fourth Annual IEEE*. 2008. IEEE.
23. Huang, R.-T., W.-J. Sheu, and C.-C. Wang, *Heat transfer enhancement by needle-arrayed electrodes–An EHD integrated cooling system.* energy Conversion and Management, 2009. **50**(7): p. 1789-1796.
24. Gallandat, N. and J.R. Mayor, *Novel Heat Sink Design Utilizing Ionic Wind for Efficient Passive Thermal Management of Grid-Scale Power Routers.* Journal of Thermal Science and Engineering Applications, 2015. **7**(3): p. 031004.
25. Jewell-Larsen, N., H. Ran, Y. Zhang, M. Schwiebert, K.H. Tessera, and A. Mamishev. *Electrohydrodynamic (EHD) cooled laptop*. in *Semiconductor Thermal Measurement and Management Symposium, 2009. SEMI-THERM 2009. 25th Annual IEEE*. 2009. IEEE.
26. Robinson, M., *Movement of air in the electric wind of the corona discharge.* American Institute of Electrical Engineers, Part I: Communication and Electronics, Transactions of the, 1961. **80**(2): p. 143-150.
27. Rickard, M., D. Dunn-Rankin, F. Weinberg, and F. Carleton, *Maximizing ion-driven gas flows.* Journal of Electrostatics, 2006. **64**(6): p. 368-376.
28. Moon, J.-D., D.-h. Hwang, and S.-T. Geum, *An EHD gas pump utilizing a ring/needle electrode.* IEEE Transactions on Dielectrics and Electrical Insulation, 2009. **16**(2): p. 352-358.
29. June, M.S., J. Kribs, and K.M. Lyons, *Measuring efficiency of positive and negative ionic wind devices for comparison to fans and blowers.* Journal of Electrostatics, 2011. **69**(4): p. 345-350.
30. Kalman, H. and E. Sher, *Enhancement of heat transfer by means of a corona wind created by a wire electrode and confined wings assembly.* Applied Thermal Engineering, 2001. **21**(3): p. 265-282.
31. Rashkovan, A., E. Sher, and H. Kalman, *Experimental optimization of an electric blower by corona wind.* Applied Thermal Engineering, 2002. **22**(14): p. 1587-1599.
32. Komeili, B., J. Chang, G. Harvel, C. Ching, and D. Brocilo, *Flow characteristics of wire-rod type electrohydrodynamic gas pump under negative corona operations.* Journal of Electrostatics, 2008. **66**(5): p. 342-353.
33. Takeuchi, N. and K. Yasuoka, *Efficiency of a wire-rod type electrohydrodynamic gas pump under negative corona operation.* IEEE Transactions on Plasma Science, 2009. **37**(6): p. 1021-1026.
34. Moreau, E. and G. Touchard, *Enhancing the mechanical efficiency of electric wind in corona discharges.* Journal of Electrostatics, 2008. **66**(1): p. 39-44.
35. Karpov, S. and I. Krichtafovitch. *Electrohydrodynamic flow modeling using FEMLAB*. in *Excerpt from the Proceedings of the COMSOL Multiphysics User's Conference 2005 Boston*. 2005.
36. Feng, J.Q., *Application of Galerkin finite-element method with Newton iterations in computing steady-state solutions of unipolar charge currents in corona devices.* Journal of Computational Physics, 1999. **151**(2): p. 969-989.
37. Peek, F.W., *Dielectric phenomena in high voltage engineering*. 1920: McGraw-Hill Book Company, Incorporated.
38. Jewell-Larsen, N.E., G.G. Joseph, and K.A. Honer. *Scaling laws for electrohydrodynamic air movers*. in *ASME/JSME 2011 8th Thermal Engineering Joint Conference*. 2011. American Society of Mechanical Engineers.
39. Feng, J.Q., *Electrohydrodynamic flow associated with unipolar charge current due to corona discharge from a wire enclosed in a rectangular shield.* Journal of Applied Physics, 1999. **86**(5): p. 2412-2418.
40. Jewell-Larsen, N.E., S.V. Karpov, I.A. Krichtafovitch, V. Jayanty, C.-P. Hsu, and A.V. Mamishev. *Modeling of corona-induced electrohydrodynamic flow with COMSOL multiphysics*. in *Proc. ESA Annual Meeting on Electrostatics, Paper E*. 2008.
41. Jewell-Larsen, N., C. Hsu, I. Krichtafovitch, S. Montgomery, J. Dibene, and A.V. Mamishev, *CFD analysis of electrostatic fluid accelerators for forced convection cooling*. Dielectrics and Electrical Insulation, IEEE Transactions on, 2008. **15**(6): p. 1745-1753.
42. Ramadhan, A., N. Kapur, J. Summers, and H. Thompson, *Numerical modelling of electrohydrodynamic airflow induced in a wire-to-grid channel.* Journal of Electrostatics, 2017. **87**: p. 123-139.
43. Kaptsov, N., *Elektricheskie yavleniya v gazakh i vakuume.* Moscow, OGIZ, 1947.
44. Abdel-Salam, M., M. Nakano, and A. Mizuno, *Corona-induced pressures, potentials, fields and currents in electrostatic precipitator configurations.* Journal of Physics D: Applied Physics, 2007. **40**(7): p. 1919.

Abdulmajeed A. Ramadhan was born in Heet, Iraq in 1978. He received the B.S. and M.S. degrees in mechanical engineering from the University of Anbar, Iraq, in 2000 and 2005, respectively, and is currently pursuing the Ph.D. degree in mechanical engineering at University of Leeds, UK. From 2006 to 2012, he worked as a lecturer in the Department of Mechanical Engineering, University of Anbar. His research interests include a wide range of topics in fluid mechanics and convection heat transfer, the applications of electrohydrodynamic flow, microelectronics cooling and thermal management.

Nikil Kapur was born in Morecambe, England in 1972. He received a BEng in chemical engineering from the University of Bradford, UK in 1994 followed by a PhD from the School of Mechanical Engineering at the University of Leeds, UK, in 1999, where he is Professor of Applied Fluid Mechanics. Prof. Kapur has authored nearly 100 papers spanning a diverse range of fluid mechanic related subjects including in manufacturing, printing, reactor designs, microfluidics and the flow and rheology of a diverse range of complex materials.

Jonathan L. Summers was born in Canterbury, Kent, England in 1964. He received a BSc and PhD degrees in applied mathematics from the University of Leeds in 1987 and 1991 respectively. He is currently a senior lecturer in Thermofluids in the School of Mechanical Engineering, University of Leeds and Research Leader at RISE SICS North in Lulea, Sweden, which has a strong focus on data centre cooling research. He is the co-author of numerous articles on the topic of thermal management of microelectronic systems, in particular the use of liquids as the prime and only cooling medium.

Harvey M. Thompson was born in Newcastle Upon Tyne, England in 1966. He received a BA in Mathematics from the University of Cambridge, UK, in 1988 and a Ph.D. from the University of Leeds, UK, in 1992. He is Head of School and Professor of Computational Fluid Dynamics in the School of Mechanical Engineering at the University of Leeds, UK. He is a Fellow of the Institution of Mechanical Engineers and has written over 150 papers and graduated more than 30 PhD students in the areas of heat and mass transfer and in CFD-based design optimisation.